# Enhanced anti-biofilm and anti-protein adsorption properties of liquid-infused silver-polytetrafluoroethylene coatings

Zhang, Shuai; Liang, Xinjin; Teng, Xiao; Gadd, Geoffrey M.; McGrath, John W.; McCoy, Coin P.

*Published in:*
Applied Surface Science

*DOI:*
10.1016/j.apsusc.2023.156463

*Publication date:*
2023

Applied Surface Science 616 (2023) 156463

Contents lists available at ScienceDirect

Applied Surface Science

journal homepage: www.elsevier.com/locate/apsusc

Full Length Article

# Enhanced anti-biofilm and anti-protein adsorption properties of liquid-infused silver-polytetrafluoroethylene coatings

Shuai Zhang [a,*], Xinjin Liang [b,c], Xiao Teng [a], Geoffrey M. Gadd [c,d], John W. McGrath [e], Coin P. McCoy [a], Qi Zhao [f]

[a] School of Pharmacy, Queen's University Belfast, BT9 7BL Belfast, UK
[b] School of Mechanical and Aerospace Engineering, Queen's University Belfast, BT9 5AG Belfast, UK
[c] School of Life Sciences, University of Dundee, DD1 5EH Dundee, UK
[d] State Key Laboratory of Heavy Oil Processing, Beijing Key Laboratory of Oil and Gas Pollution Control, China University of Petroleum, Beijing 102249, China
[e] School of Biological Sciences, Queen's University Belfast, Belfast BT9 5DL, UK
[f] School of Science and Engineering, University of Dundee, DD1 4HN Dundee, UK

ARTICLE INFO

*Keywords:*
Silver
Polytetrafluoroethylene
Bacteria
Coating
Biofilm
Protein

ABSTRACT

In this work, a slippery liquid-infused silver-polytetrafluoroethylene (AgFP) coating was fabricated *via* a spontaneous polycondensation of 1H,1H,2H,2H-perfluorooctyltriethoxysilane (PFOTES) onto an electroless AgF sublayer. The AgFP coating demonstrated great stability and superior repellence against liquids with a wide range of surface tensions. The anti-biofouling properties were investigated by adsorption of *Escherichia coli*, *Staphylococcus aureus*, fibrinogen, and bovine serum albumin. Owing to the self-cleaning property, the AgFP demonstrated enhanced anti-adhesion activity against both bacteria and proteins relative to traditional electroless coatings, despite the fibrinogen deposition significantly promoting bacterial binding. While its ultra-low surface energy was not within the optimum surface energy region for minimum bacterial or protein adhesion, the AgFP coating still displayed excellent anti-biofilm capability in a protein-bacteria co-deposition model, reducing over 80% of BSA-supplemented biomass coverage on Ag surfaces and over 60% of Fgn-supplemented biomass coverage on AgF surfaces, respectively. To understand the anti-adhesion mechanism, the XDLVO model was used to explain the adhesion behaviour of both bacteria and proteins. Cytotoxicity assays confirmed that the AgFP coating had good biocompatibility with fibroblast cells. The results from this research provide attractive prospects for the application of the AgFP coating in biomedical devices to combat infections.

## 1. Introduction

Medical device-associated infections (MDIs) remain a major concern globally. As a basic survival strategy, microorganisms tend to colonise and grow on surfaces rather than exist as individual organisms in a 'planktonic state' [1]. Current strategies to prevent MDIs mainly include antimicrobial, anti-adhesive, and combinatorial approaches, all of which have achieved great success over recent decades [2–4]. The antimicrobial approach works through killing or inhibiting the growth of microbes using various types of antimicrobial agents [5–10], but only silver and a few types of antibiotics have entered clinical use to date, where their limited long-term efficacy and the emergence of silver/antibiotic-resistant pathogenic bacteria remain to be addressed [11]. Anti-adhesion surfaces prevent microbial adhesion and retard biofilm formation by incorporating topographical features or low surface energy chemistry to enhance surface repellency. These surfaces are generally considered superhydrophobic or superoleophobic and are superrepellent to liquids (water and oil, respectively). However, their long-term use in biomedical applications remains challenging because of the fragile micro/nanostructures involved [12,13].

Theoretically, initial adhesion of bacteria to surfaces can be predicted and explained by the extended Derjaguin-Landau-Verwey-

*Abbreviations:* SLIS, slippery liquid-infused surface; PFOTES, 1H,1H,2H,2H-perfluorooctyltriethoxysilane; OSE, optimum surface energy; Ag-PTFE or AgF, silver-polytetrafluoroethylene; AgFP, PFOTES modified silver-polytetrafluoroethylene; Fgn, fibrinogen; BSA, bovine serum albumin; XDLVO, extended Derjaguin-Landau-Verwey-Overbeek; CA, contact angle; CAH, contact angle hysteresis.

* Corresponding author.
*E-mail address:* shuai.zhang@qub.ac.uk (S. Zhang).

https://doi.org/10.1016/j.apsusc.2023.156463
Received 27 October 2022; Received in revised form 27 December 2022; Accepted 14 January 2023
Available online 20 January 2023

Overbeek (XDLVO) theory [14]. Bacteria, seen as inert colloidal particles, reach the proximity of a surface and become reversibly attached, the process being governed by a range of distance-dependent physicochemical interactions [15]. According to the XDLVO model, the surface free energy and its components of a solid surface can significantly influence van der Waals and acid-base interactions, affecting bacterial adhesion at both long- and short-range [16]. Baier first reported that there exists an optimum region of surface energies where bacterial adhesion is minimal and this finding has been extensively verified over subsequent decades [17–19]. Inspired by this, Zhao developed an electroless silver-polytetrafluoroethylene (Ag-PTFE or AgF) coating with tailored surface energy for medical devices and reported that the optimum surface energy (OSE) for minimum bacterial adhesion was about 24.5 mN/m [20,21]. However, on exposure to a complex physiological environment, proteins may rapidly adsorb onto device surfaces and redefine the surface properties, acting as a conditioning film and regulating subsequent bacterial adhesion through specific protein-bacterial interactions [22,23]. The deposition of certain types of host serum proteins can even promote bacterial colonisation and biofilm formation [24]. Despite PTFE being a well-known non-stick material, serum proteins have been shown to rapidly saturate the surfaces of PTFE *via* hydrophobic interactions and spread their hydrophobic core over the surface, resulting in high protein retention [25,26]. To date, the anti-protein adsorption performance of Ag-PTFE coatings has not been reported and their anti-biofilm properties in the presence of proteins remain to be investigated.

On the other hand, the emergence of slippery liquid-infused surfaces (SLIS) has attracted considerable interest due to their excellent self-cleaning properties. Compared with traditional surfaces, the SLIS inspired by *Nepenthes* pitcher plants can eliminate pinning of the liquid contact line and enhance drop mobility, providing enhanced repellence towards a range of liquids and biomolecules, thus showing great promise in preventing protein adsorption [27,28]. However, recent studies revealed that the passive liquid-infused surface alone was unable to provide long-term protection against bacterial contamination as certain types of bacteria can form 'beachheads' colonies within the lubricant layer, enabling bacterial colonisation, proliferation, and biofilm formation [29]. To account for the above limitations, the combination of SLIS and the antibacterial AgF could exhibit a synergy resulting in medical devices with enhanced anti-biofilm and anti-protein adsorption.

According to Aizenberg [30], the two primary features that are required to create SLIS include the capacity for physical entrapment of a lubricating film within a nanostructured solid substrate and high chemical affinity between the film and solid. 1H,1H,2H,2H-perfluorooctyltriethoxysilane (PFOTES) is a fluorinated alkyl silane that can hydrolyse and develop into a silane-based film through continuous polycondensation, which has been widely used in synthesising liquid-repelling surfaces due to its ultralow surface energy [31–33]. In our design, benefiting from the incorporated PTFE particles, a lubricating fluoropolymer layer derived from self-assembling polycondensation of PFOTES was infused into the surface texture of the AgF coating to strengthen the anti-protein adsorption activity. The association between the wettability of the liquid-infused AgF coating (AgFP) and surface topography was investigated in detail. The stability and durability of the AgFP coatings were assessed under dynamic conditions for up to 7 days. Protein and bacterial attachment to the fabricated coatings was examined and compared with uncoated stainless steel (SS), Ag, and AgF coatings using a protein-bacteria co-deposition model. The relationship between protein adsorption and biofilm formation is discussed and explained using the XDLVO model.

## 2. Materials and methods

### 2.1. Materials

Medical grade 304 stainless steel sheets were purchased from Goodfellow Ltd. (Cambridge, UK) and cut into disks with a diameter of 1 cm. LIVE/DEAD BacLight Bacterial Viability Kit L13152, Alexa Fluor™ 488 Phalloidin, and DAPI (4′,6-Diamidino-2-Phenylindole, Dihydrochloride) were purchased from Thermo Fisher Scientific (Paisley, UK). *Escherichia coli* NCTC 11560 *(E. coli)* and *Staphylococcus aureus* NCTC 12,493 *(S. aureus)* were obtained from the School of Biological Sciences, Queen's University Belfast (Belfast, UK). Other chemicals used in this study were purchased from Merck Life Science UK Ltd. (Dorset, UK) without further purification.

### 2.2. Coating preparation

Prior to electroless plating, the disks were electrochemically polished followed by surface activation using our previously reported method [34,35]. The obtained disks were vertically immersed in a plating bath for 30 min at room temperature. The silver plating bath comprised $AgNO_3$ 3.0 g/L, $KNaC_4H_4O_6{\cdot}4H_2O$ 25 g/L, $C_4H_6O_6$ 0.5 g/L, $C_2H_5OH$ 5 mL/L and $NH_3{\cdot}H_2O$ 0.1 M. To incorporate PTFE into the coating matrix, PTFE emulsion (60 w/w%) with suitable surfactants was added into the plating bath at concentrations of 5 to 20 mL/L. The obtained Ag coatings and AgF coatings were sequentially rinsed with 2.0% (v/v) $HNO_3$, deionised water, and ethanol and air-dried at room temperature. To prepare AgFP coatings, the prepared samples were immersed in PFOTES solution (0–30 v/v%) for 48 h at 60 rpm at room temperature. The samples were then removed and sequentially rinsed with ethanol, deionised water, and acetone, and stored at room temperature before use.

### 2.3. Characterisation

Scanning electron microscopy (FE-SEM, JSM-6500F, JEOL, Tokyo, Japan) and atomic force microscopy (AFM, Cypher, Oxford Instruments, Oxford, UK) were used to examine the morphological features of the coatings. Surface chemistry composition was analysed by energy-dispersive X-ray spectrometry (EDX, X-Stream-2/micsF+, Oxford Instruments, Oxford, UK). ImageJ (LOCI, University of Wisconsin, Wisconsin, USA) was used to identify the PTFE particles and their size distribution was calculated from three random SEM images. The absorption spectra of the coatings were obtained using Fourier transform infrared spectroscopy (FTIR) using a Spectrum Two spectrometer (PerkinElmer, Shelton, USA) with the wavenumber ranging from 650 to 4000 $cm^{-1}$. Contact angles (CAs) were measured using a sessile drop method at room temperature with a tensiometer (Theta Flow, Bolin Scientific, Sweden) and the surface free energy was calculated using the van Oss method [36]. The advancing and receding CAs were also obtained while the probe fluid was added to and withdrawn from the drop, respectively. The release profile of silver ions ($Ag^+$) was monitored by immersing each sample in 1 mL PBS for up to 7 days and the concentration of free $Ag^+$ was determined using inductively coupled plasma optical emission spectrometry (ICP-OES, Agilent 5100, Santa Clara, USA).

### 2.4. Stability tests

To investigate the durability of the coatings in an aqueous system, the samples (n = 3) were vertically immersed in PBS at 100 rpm for up to 7 days at 37 °C. To assess their stability under shear stress, the samples were spun from 500 to 6000 rpm in PBS for 1 min. The change in contact angle hysteresis (CAH) was monitored and the coating integrity was assessed by optical microscopy.

### 2.5. Protein adsorption assay

The samples (n = 3) were immersed into 2 mL of Fgn (1 mg/mL) and BSA solutions (50 mg/mL) at 37 °C at 100 rpm. After 24 h, the samples were removed from the solutions and gently washed three times with

PBS followed by ultrasonication (60 kHz) in 1 mL of 5 wt% sodium dodecyl sulfate (SDS) for 60 min. Complete removal of protein was confirmed by SEM. The protein concentration was determined by the Bicinchoninic acid (BCA) method [37]. Briefly, 25 μL of the obtained protein solution was thoroughly mixed with 200 μL working reagent and incubated at 37 °C for 30 min. The absorption at 562 nm was determined by UV–vis spectrophotometry and the amount of adsorbed protein on each sample was calculated. Six measurements were performed for each sample.

### 2.6. Bacterial adhesion and anti-biofilm assays

A single bacterial colony of *E. coli* or *S. aureus* was inoculated into 20 mL tryptic soy broth (TSB) and grown overnight in a shaking incubator at 150 rpm at 37 °C. To achieve the best adhesion, 100 μL of the bacterial culture was transferred to 10 mL fresh TSB and grown to the mid-logarithmic phase, and subsequently centrifuged and diluted to ~$10^7$ CFU/mL with PBS. The samples (n = 3) were immersed in 2 mL of the above bacterial suspension and incubated at 100 rpm at 37 °C for 24 h. The number of attached bacteria was quantified by plate counting [38]. To investigate the influence of protein adsorption on biofilm formation, the samples (n = 3) were incubated with 2 mL of protein-supplemented bacterial suspension (~$10^8$ CFU/mL, 50 mg/mL BSA or 1 mg/mL Fgn) for 24 h and the sample surfaces directly examined using a fluorescence microscope. A LIVE/DEAD Baclight bacterial viability kit L13152 comprising green-fluorescent SYTO® 9 stain and red-fluorescent propidium iodide was used to stain the living (green) and dead (red) bacteria, respectively. The surface coverage of biofilm on each surface was determined and calculated using Image J.

### 2.7. Cytotoxicity assays

*In vitro* cytotoxicity against mouse fibroblast cells L929 (ECACC 85011425) and human foetal osteoblasts (hFOBs 1.19) was assessed by a direct contact approach and the cell viability was determined *via* an MTT method. In brief, the L929 cells at a density of 5 × $10^4$ cells/well were seeded in a 48-well plate and cultured in supplemented EMEM (10% FBS, 100 mg/mL penicillin, and 100 mg/mL streptomycin) for 24 h to enable cell adhesion. The media in each well were then removed and the sterilised samples (n = 6) were carefully placed in the wells followed by adding 1 mL of fresh media. After 1 and 3 days, the media and samples were removed, and 100 μL of 3-(4,5-dimethylthiazol-2-yl)-2,5-diphenyltetrazolium bromide was added to each well and incubated for 4 h followed by the addition of 1 mL of isopropanol to dissolve the formazan. The absorbance was measured at 570 nm and relative cell viability was measured by comparison with the negative control (wells containing no samples). Cells in additional wells (n = 3) on day 3 were stained with Alexa Fluor 488 phalloidin and DAPI according to manufacturer's instructions and their morphologies were observed using a fluorescence microscope (Nikon 6D Live Cell Imaging Inverted Microscope, Nikon, Tokyo, Japan).

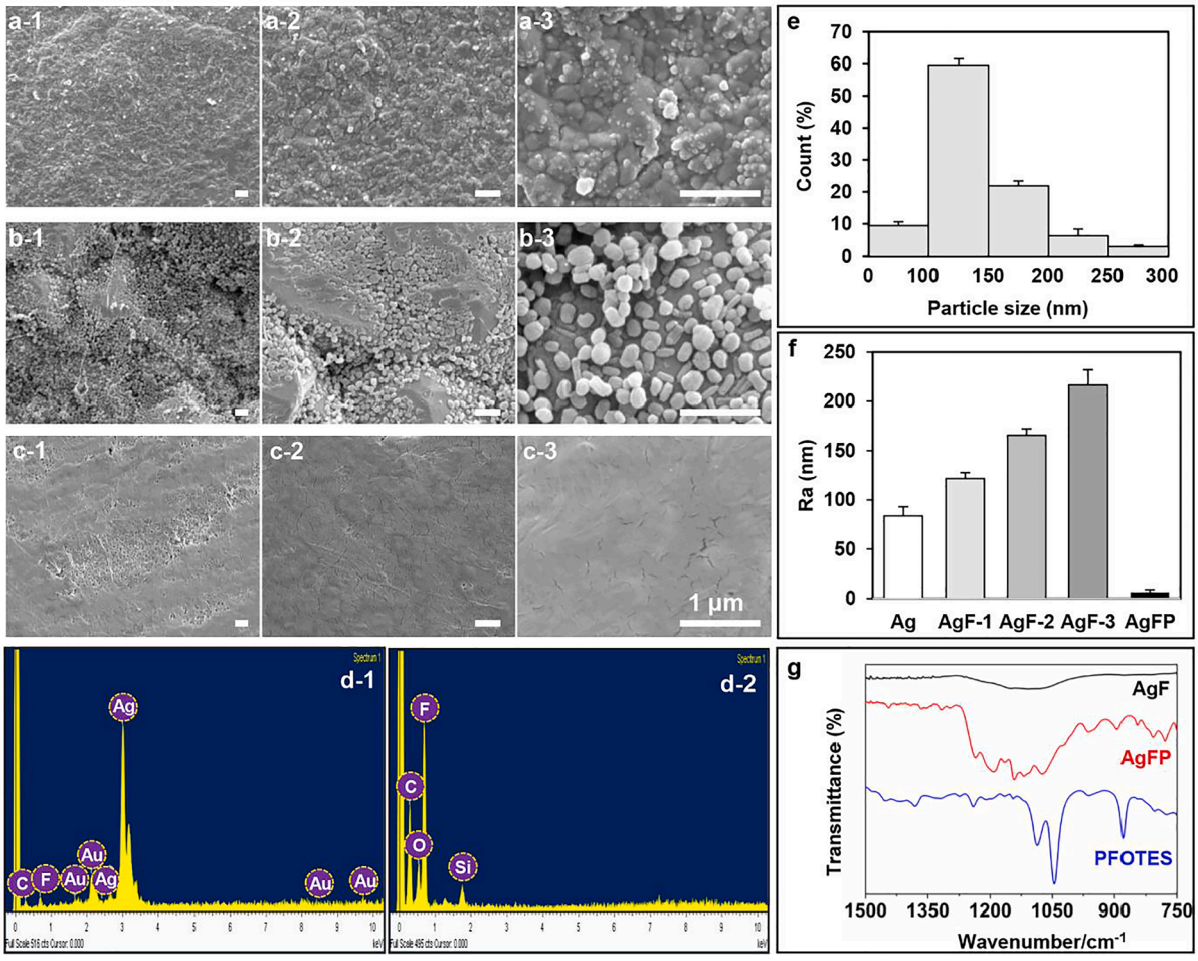


**Fig. 1.** Typical SEM images of (a) Ag, (b) AgF, and (c) AgFP coatings (scale bars correspond to 1 μm); typical EDX spectrum of the (d-1) AgF and (d-2) AgFP coatings; (e) size distribution of the PTFE particles; (f) surface roughness (Ra); (g) FTIR spectra (n = 3, bars represent standard deviation of the mean).

### 2.8. Statistical analysis

All data are presented as the means ± standard deviation. A one-way ANOVA (Tukey's post hoc) was performed to determine statistical significance where values of $p < 0.05$ were considered significant and $p < 0.01$ were considered highly significant.

## 3. Results and discussions

### 3.1. Surface characterisation

Fig. 1a, b, and c show the typical surface morphologies of the Ag, AgF, and AgFP coatings, respectively. In comparison with the AgF coating, the neat Ag coating showed a dense and smoother surface with a silver grain size in the range of ~70 nm to 150 nm. The weak reducer ($KNaC_4H_4O_6{\cdot}4H_2O$) in the plating bath effectively reduced the growth rate of silver crystal particles and produced a fine-grained silver coating with low porosity. The co-deposition of PTFE particles resulted in the formation of large polygonal silver hillocks (Fig. 1b-1 and Fig. 1b-2) as the PTFE particles disrupted the silver crystal lattice and impeded the 3D growth of surrounding silver islands, leading to continuous crystal accumulation in other directions. Owing to the presence of surfactants, the PTFE particles were uniformly distributed within the silver matrix with an average particle size of ~100 to 150 nm (Fig. 1e). The increased PTFE concentration (from 5 to 20 mL/L) in the plating bath did not induce aggregation of PTFE particles but resulted in a significant increase in surface roughness (Fig. 1f). As shown in Fig. 1c, the AgFP coating exhibited the smoothest surface with an arithmetical mean roughness (Ra) value of ~6 nm. The void gaps were occupied and covered by a flat layer, and the chemical composition of the overlayer was analysed by EDX and FTIR. As seen in Fig. 1d-1, the EDX spectrum of the AgF coating showed three main peaks (Ag, C, and F) with the maximum peak intensity for Ag while that of the AgFP coating demonstrated additional peaks (O and Si) and significantly higher levels of C and F (Fig. 1d-2). The loss of the Ag peak indicated that the AgF coating was fully covered with the lubricating layer and the O, Si, C, and F originated from the PFOTES and/or its hydrolysates. It could be speculated that its thickness was at least 1 μm considering the penetration depth of the electron beam under 10 keV [39]. Fig. 1g shows the FTIR spectra of the PFOTES, AgFP, and AgF coating. Both PFOTES and the AgFP coating exhibited characteristic C-F, $CF_2$, and $CF_3$ peaks at 1240, 1143, and 1165 $cm^{-1}$. The bare PFOTES displayed clear Si-O-C peaks at 1044 and 1086 $cm^{-1}$, but these two peaks were not evident in the AgFP coating. Instead, the AgFP coating exhibited two new peaks at 1074 and 1120 $cm^{-1}$, respectively, which were attributed to the polymerised siloxane network Si-O-Si [40]. Upon hydrolysis, the ethoxy group of the PFOTES can react with water to form hydrolysed siloxanes and bond with other molecules comprising hydrolysed siloxanes, forming a larger fluoro-molecule *via* continuous condensation. These fluoro-molecules could be locked within the surface textures of the AgF coating due to the high chemical affinity to PTFE.

The wetting behaviour of the coatings was investigated by measuring the static CA, advancing angle, and receding angle, as well as the CAH on different surfaces with diverse liquids. As seen in Fig. 2, the Ag coating was readily wetted by all types of liquids. The incorporation of PTFE into the Ag coating significantly reduced its surface energy (Table 1), resulting in increased repellency against water (72.8 mN/m), diiodomethane (50.8 mN/m), and ethylene glycol (48 mN/m) but not low-surface-tension liquids such as ethanol (21.8 mN/m). This is because the rough surface texture of the AgF coating in fact allows for wetting behaviour in the Wenzel state despite the AgF-3 coating having even lower surface energy (17.2 mN/m) according to Young's equation (Table 1). Similar results were also obtained with the AgFP coating, suggesting that its smooth surface morphology and ultralow surface energy (12.8 mN/m) did not inhibit wetting by ethanol. As shown in Fig. 1g, the peaks at 894 and 962 $cm^{-1}$ indicated the unreacted silanol groups Si-OH on the AgFP coating, which could absorb ethanol through hydrogen-bonding interactions and promote surface wetting [33]. Nonetheless, the AgFP coating exhibited broad liquid repellency as signified by very low contact angle hysteresis (CAH, 2.6 ° to 5.8 °) (Fig. 3a) against liquids of surface tensions ranging from 21.8 mN/m (ethanol) to 72.8 mN/m (water). The low values of CAH further confirm a lack of pinning, consistent with a slippery and defect-free surface (Fig. 1c). Based on the measured advancing/receding angle and droplet volume (3 μL), the estimated liquid retention force [41] for the above-mentioned liquids on the AgFP coating is 2.67 ± 0.39 μN, which is more than an order magnitude less than that on the AgF-3 coating (30.82 ± 5.14 μN). To verify this, the mobility of water droplets (20 μL) on the AgF and AgFP coatings was investigated. As shown in Movie 1, the AgFP coating exhibited outstanding water repellency as evidenced by

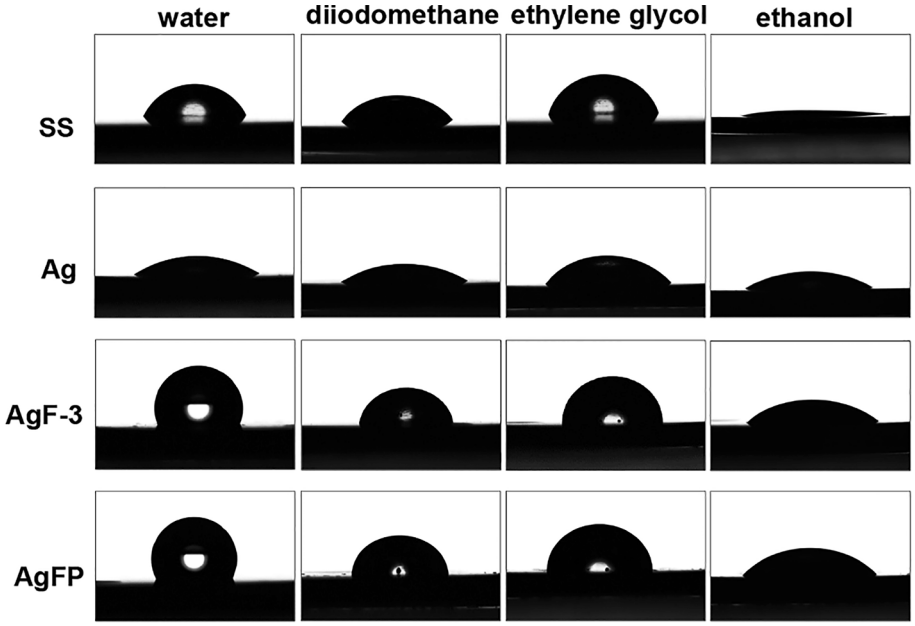


**Fig. 2.** The repellency of different surfaces to diverse liquids.

**Table 1**
Contact angle and surface free energy of different surfaces.

| Samples | Particle conc. (g/L) PTFE | Contact angle, $\theta$ (deg) $\theta^W$ | $\theta^D$ | $\theta^E$ | Surface free energy (mN/m) $\gamma^{LW}$ | $\gamma^+$ | $\gamma^-$ | $\gamma^{TOT}$ |
|---|---|---|---|---|---|---|---|---|
| SS | | 65.2 ± 1.0 | 54.9 ± 0.5 | 71.0 ± 2.1 | 31.50 | 0.98 | 16.46 | 39.52 |
| Ag | | 30.4 ± 1.8 | 32.5 ± 0.1 | 51.5 ± 1.1 | 43.16 | 1.47 | 37.71 | 58.03 |
| AgF-1 | 5.0 | 77.9 ± 1.6 | 63.3 ± 2.2 | 76.1 ± 1.7 | 26.68 | 0.41 | 10.90 | 30.92 |
| AgF-2 | 10.0 | 98.8 ± 2.0 | 72.5 ± 2.5 | 82.0 ± 3.1 | 21.49 | 0.00 | 3.22 | 21.58 |
| AgF-3 | 20.0 | 113.8 ± 1.9 | 80.9 ± 2.7 | 89.8 ± 1.5 | 17.03 | 0.05 | 0.07 | 17.15 |
| AgFP | 20.0 | 115.4 ± 2.4 | 90.2 ± 1.8 | 89.4 ± 0.6 | 12.61 | 0.53 | 0.01 | 12.77 |
| BSA | | 50.2 ± 3.7 | 34.8 ± 1.1 | 14.8 ± 2.9 | 42.12 | 0.59 | 25.56 | 49.86 |
| Fgn | | 68.7 ± 1.2 | 31.9 ± 1.5 | 48.2 ± 0.6 | 43.42 | 0.01 | 13.07 | 44.34 |
| *E. coli* | | 16.5 ± 1.1 | 47.6 ± 0.5 | 22.9 ± 0.7 | 35.60 | 0.14 | 67.68 | 41.76[56] |
| *S. aureus* | | 16.6 ± 1.8 | 54.8 ± 0.7 | 22.3 ± 1.2 | 31.56 | 0.43 | 68.32 | 42.40[56] |

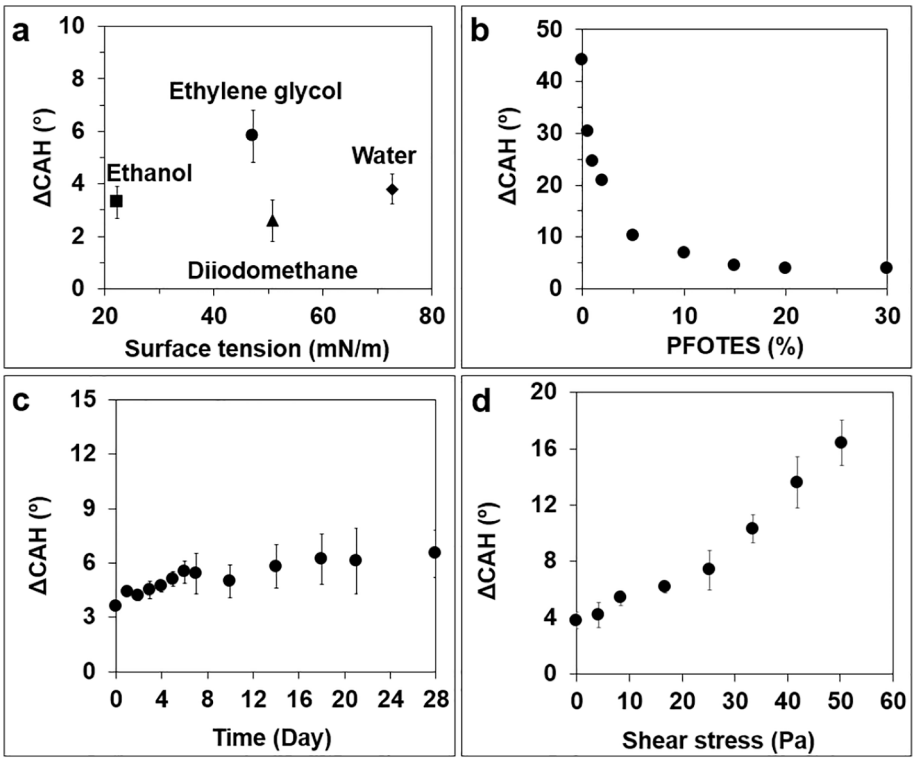


**Fig. 3.** (a) the CAHs ($\Delta\theta$) of diverse liquids on the AgFP coating; (b) variations of the water CAH ($\Delta\theta$) on the AgFP coating and the corresponding amount of PFOT; comparison of the CAHs ($\Delta\theta$) of water measured on the AgFP coatings after (c) immersing in PBS for up to 28 days and (e) spinning in PBS for 1 min with shear stress (CAH: contact angle hysteresis, n = 3, bars represent standard deviation of the mean).

immediate flowing away of the water droplet whilst the AgF coating displayed significant water retention due to the microtextural roughness (Movie 2). The adhesion and retention of liquid droplets might indicate a potential cause of bacterial contamination [42].

Fig. 3b shows the influence of PFOTES concentration on water repellence, and the CAH values were calculated and used as a qualitative indicator. PFOTES could self-assemble into complex fluorinated structures *via* self-polycondensation reactions and occupy the hierarchical microscale structures and void gaps, leading to a flat and smooth liquid-like surface (Fig. 1c). The increased PFOTES level in the coating bath in fact led to a higher surface coverage over the AgF sublayer, exhibiting lower resistance to water mobility. To investigate the stability and durability, the samples were subjected to long-term immersion in PBS and high centrifugal forces. For the immersion test, the samples were vertically immersed in PBS and flushed at an estimated speed of 6 cm/s for up to 28 days. The water CAHs slightly decreased with time but remained at a low value of ~6.5 ° (Fig. 3c). Microscopic observations confirmed that the AgFP surface retained its integrity after 28 days. For the centrifuge test, the samples were centrifuged by increasing spin rates from 500 to 6000 rpm for 1 min. As seen in Fig. 3d, following centrifugation below 1000 rpm (i.e., a shear stress of 8.4 Pa according to Newton's law [43]), the CAH values remained about 5 °. With increased spinning rate, the CAHs gradually increased due to the loss of the liquid layer, reaching ~10 ° at 4000 rpm (33.5 Pa). Under high spin rates over 5000 rpm, exposure of the underlying nanostructures was observed and the CAH values increased to ~16 ° at 6000 rpm (50.3 Pa). Compared with the AgF surface (CAH ~44 °), these results indicate that AgFP surfaces possess excellent stability and durability in an aqueous system even under high shear conditions. According to literatures [44,45], for indwelling urinary catheters, the flow-induced shear stress ranges from 0.3 to 0.5 Pa in the urethra, and for vascular stents, the maximum time-averaged levels of shear stress are around 3.0 Pa in the arterial circulation. Taken together, the AgFP coating was shear stable and nearly no difference in CAH was noticed below 4 Pa, indicating the AgFP coating could be potentially applied for medical devices (e.g., urinary catheters and vascular stents).

### 3.2. Bacterial adhesion

Despite Ag-releasing coatings gaining popularity in preventing MDIs, neat Ag coatings often fail to provide long-term protection against bacterial adhesion due to insufficient $Ag^+$ release. In an attempt to overcome this limitation, the AgF coating combines both active anti-bacterial silver and passive anti-adhesive PTFE to impede bacterial adhesion. Upon immersing in PBS, the AgF coating (AgF-2) demonstrated a lower but similar $Ag^+$ release profile as compared with the Ag coating (Fig. 4a). This is because the smaller silver particles within the Ag coating (Fig. 1a) enabled faster oxidative dissolution of $Ag^+$ and the enhanced surface hydrophobicity of AgF coating impeded water-surface interactions. After 3 days' release, a new stable surface state was built with subvalent silver, yielding a slower but sustained $Ag^+$ release [46]. In comparison, the AgFP coating exhibited a nearly constant but significantly lower level of $Ag^+$ release over the whole test period, presumably because the liquid-like overlayer impeded water to penetrate and contact with the underlying silver matrix. To determine the total loading amount of silver in coatings, the coated samples were immersed in 5% $HNO_3$ until the coating was fully dissolved. The solution was filtered, the silver concentration was determined by ICP and the total amount of silver was calculated. For the neat Ag coating, the silver loading was ~0.76 mg/cm$^2$. For the AgF-2 coating, the silver loading was ~0.63 mg/cm$^2$. Combined with the silver release data (Fig. 4a), the neat Ag and AgF-2 coatings released 0.47 % and 0.36 % (w/w) of the total silver after 7 days, respectively. For the AgFP coating, only 0.13% of the total silver was released after 7 days.

However, it should be noted that the released $Ag^+$ even at the highest concentration was unable to kill all the bacteria in the suspensions. As evident after 24 h of co-culture with *E. coli* or *S. aureus*, the Ag and AgF surfaces still demonstrated extensive bacterial adhesion (Fig. 4b). The incorporation of PTFE particles altered the anti-adhesion efficacy after and minimum bacterial adhesion was observed when the PTFE concentration reached 10 mL/L (AgF-2), reducing 60.6% and 30.3% of *E. coli* adhesion, 51.9% and 22.1% of *S. aureus* adhesion, respectively, when compared with SS and Ag coating. These results are consistent with our previous findings [20]. Notably, a further ~70% reduction in CFU was observed on the AgFP coating regardless of its weakest anti-bacterial activity. Generally, 24 h is the early time point of biofilm formation [47] and the results suggest that the liquid-like AgFP surface could effectively reduce bacterial accumulation and inhibit biofilm formation.

### 3.3. Protein adhesion

For medical devices such as catheters, stents, and orthopaedic implants, protein-surface interactions are the first step when they come in contact with biological fluids. Protein adsorption can often lead to

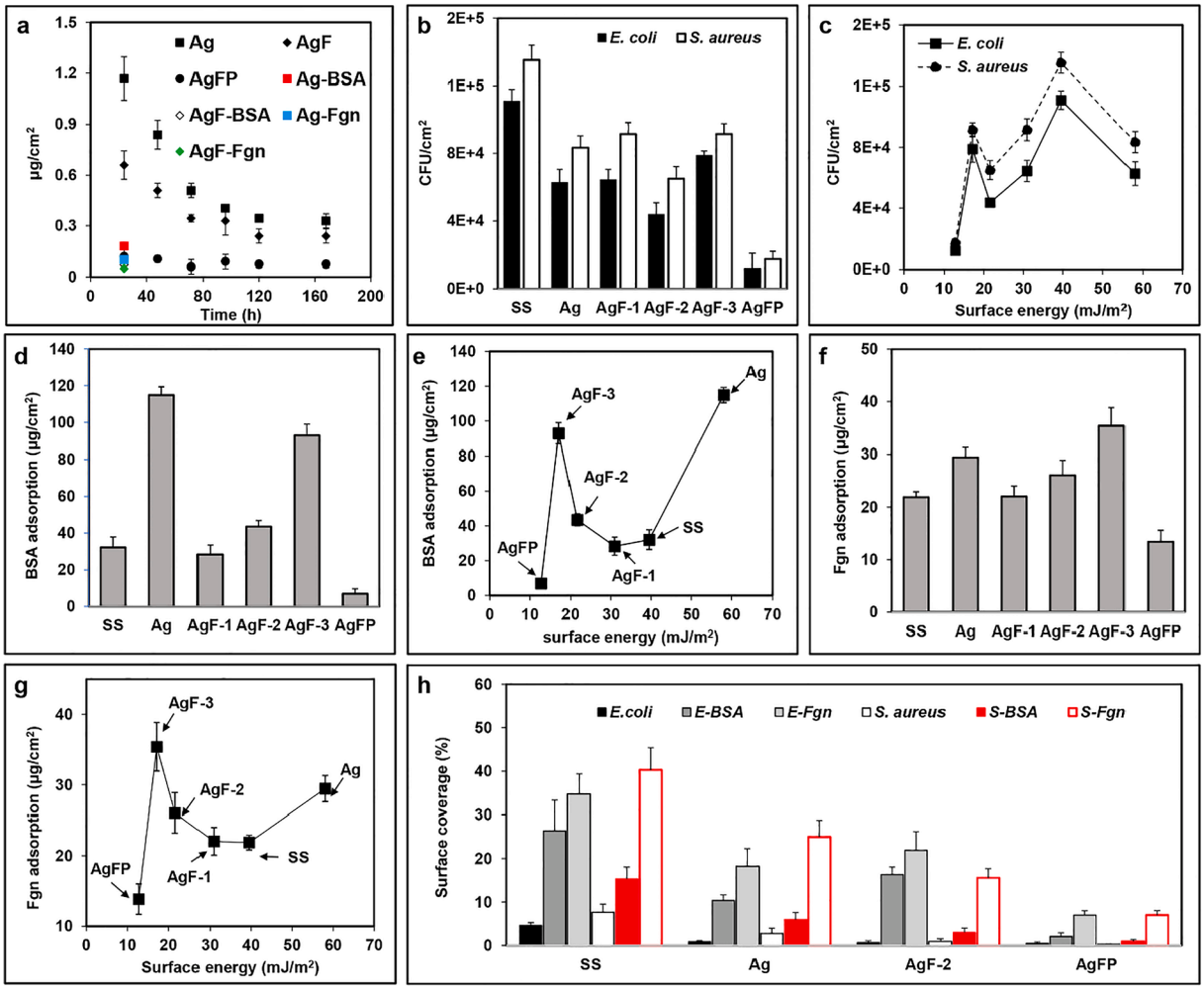


**Fig. 4.** (a) Silver release profiles from different coatings over time; (b) quantitative counts of viable bacterial cells adhering to different surfaces after 24 h of incubation; (c) the influence of total surface energy on bacterial adhesion; (d) BSA adsorption on different coatings after 24 h; (e) the influence of total surface energy on BSA adsorption; (f) Fgn adsorption on different coatings after 24 h; (g) the influence of total surface energy on Fgn adsorption; (h) comparison of surface coverage of biofilm on different coatings after 24 h (n = 6, bars represent standard deviation of the mean).

profound alterations in the surface properties, inhibiting or facilitating attachment of bacteria, or other surface-active species [48]. In this study, the protein adhesion on different surfaces was examined at pH 7.4 with two common plasma proteins, BSA and Fgn. BSA is the most abundant protein in the circulatory system with a concentration of about 50 mg/mL in blood plasma [49]. As seen in Fig. 4d, Ag and AgFP had the highest and lowest BSA absorption of 114.9 ± 4.9 and 7.0 ± 2.7 μg/cm$^2$, respectively. As evident from the surface energy analysis (Table 1), BSA (-18e at pH 7.4) would not favourably absorb onto the negatively charged Ag coating if only considering the electrostatic interactions. However, the high ionic strength of PBS (0.16 M) may screen the surface charges of both the BSA and Ag coating, reducing long-range electrostatic repulsion [50]. Previous studies also reported that BSA could strongly bind to Ag forming sulphur-silver complexes [51]. After incorporating PTFE, the coating showed overall less BSA adsorption, and a higher PTFE content resulted in increased protein adhesion. Similar phenomena were also found with Fgn while the AgF-3 had the highest Fgn attachment (Fig. 4f). The presence of PTFE enhanced the hydrophobic interactions between the hydrophobic groups of the protein and the coating, which in turn may facilitate protein binding and contribute to a higher equilibrium adsorbed amount of proteins. Moreover, the deposition of protein resulted in a dramatic decrease in silver release (Fig. 4a) with both Ag and AgF-3. The level of released $Ag^+$ after 24 h was nearly equal to that from the AgFP in pure PBS, indicating that absorbed protein hindered silver release and this may further block the interaction of antibacterial $Ag^+$ with bacteria.

### 3.4. Effect of surface energy on biofouling adhesion

Similar to bacterial adhesion, the process of protein adsorption also involves a range of long- and short-range physical interactions [49], and so the influence of surface energy of the coatings on bacterial adhesion and protein adsorption was investigated. Complied with the Baier curve, Fig. 4c shows that there exists an OSE (AgF-2, 21.58 mN/m) where adhesion is minimal. This OSE value is nearly equal to the dispersive component ($\Upsilon_w^{LW}$) for water (21.8 mN/m), which may enable water to rewet the surface at the minimised energy cost, thereby reducing the likelihood of bacterial adhesion. Interestingly, bacterial adhesion on Ag and AgFP coatings was much lower than estimations from the Baier's curve. As evident from the ICP analysis (Fig. 4a), the Ag coating released a higher level of $Ag^+$ that may kill the adhered bacteria given that only viable cells were counted. With regard to the AgFP coating, its ultra-low CAH may inhibit initial bacterial attachment and the liquid-like overlayer with ultra-low surface energy (12.8 mN/m) could eliminate the strong interactions with bacteria, enabling ease of detachment in the presence of shear stress. Similar results were also observed with protein adhesion (Fig. 4e and g), but the OSE value in the case of BSA and Fgn extended to a higher and wider region (30–40 mN/m). Zhao et al. [18] derived the optimum surface free energy for minimum protein adhesion force using the XDLVO (equation (1)):

$$\Upsilon_s^{TOT} = \frac{1}{4}\left(\sqrt{\Upsilon_p^{LW}} + \sqrt{\Upsilon_f^{LW}}\right)2 + 2\sqrt{\Upsilon_S^+}\left(\frac{\sqrt{\Upsilon_p^-\Upsilon_s^+} + \sqrt{\Upsilon_f^+\Upsilon_f^-} - \sqrt{\Upsilon_f^-\Upsilon_s^+} - \sqrt{\Upsilon_f^-\Upsilon_p^+}}{\sqrt{\Upsilon_f^+} - \sqrt{\Upsilon_p^+}}\right) \quad (1)$$

where $\Upsilon^{TOT}$, $\Upsilon^{LW}$, $\Upsilon^+$ and $\Upsilon^-$ are the total surface energy, Lifshitz-van der Waals (LW) apolar component, electron donor, and electron acceptor subcomponents (s: surface; p: protein; f: fluid). To verify the obtained OSE values with protein adsorption, the surface energy and its components of proteins were measured and calculated according to Neumann et. al [52]. By combing eq. (1) and the data from Table 1, the theoretical value of $\Upsilon_s^{LW}$ for minimum protein adhesion in pure water is about 32 mN/m, which is nearly equal to the $\Upsilon_s^{LW}$ of SS. Following this, the theoretical value of OSE value is about 41 mN/m. On the other hand, considering the screening of surface charges due to the high ionic strength, the eq. (1) may be further simplified to eq. (2):

$$\Upsilon_s^{TOT} = \Upsilon_s^{LW} = \frac{1}{4}\left(\sqrt{\Upsilon_p^{LW}} + \sqrt{\Upsilon_f^{LW}}\right) \quad (2)$$

and this may explain the wide distribution of OSE for protein adsorption.

### 3.5. Effect of protein co-deposition on bacterial adhesion

Recent findings in biliary stents [53] and urinary catheters [24] have revealed that certain types of host-derived proteins can promote bacterial colonisation and the subsequent establishment of biofilms. To mimic the complexities of the biological environment, the antibiofilm performance of the coatings was challenged with a protein-bacteria co-deposition model. The AgF-2 coating with verified best anti-adhesion performance (Fig. 4b) was used as a reference. As seen in Fig. 5, for both strains, the AgFP exhibited the best anti-adhesion efficacy in PBS with nearly no bacterial attachment. For either SS, Ag, or AgF-2 coating, only isolated bacteria were found on the surfaces, indicating biofilm was not formed at this stage. The Ag coating demonstrated a stronger bactericidal activity than the AgF-2 coating as evidenced by the greater ratio of dead cells. After introducing proteins into the media, all the surfaces experienced a dramatic increase in biofilm coverage (Fig. 4h). For *E. coli*, bacteria in large cell aggregates or clusters were observed on the SS, Ag, and AgF-2 surfaces while only sparse and isolated cells were seen on the AgFP surface. The AgFP coating reduced ~80% and ~87% of BSA-supplemented biomass coverage on Ag and AgF-2 surfaces, respectively. Interestingly, as evidenced by fluorescence results, the Fgn at a lower concentration (1 mg/mL) demonstrated a stronger capability in promoting bacterial binding than BSA (50 mg/L). For *E. coli*, the AgFP coating could still reduce ~61% and ~68% of Fgn-supplemented biomass coverage on Ag and AgF-2 surfaces, respectively. Early studies on mouse urinary catheterisation indicated that the binding of Gram-negative bacteria (such as *E. coli*) to Fgn is critical for efficient bacterial colonisation and biofilm formation as their chaperone-usher pathway (CUP) pili could bind specifically to the glycosylated portion of Fgn. Similar results were also obtained with *S. aureus*, as recent findings showed that the clumping factor A (ClfA) on the surface of *S. aureus* could promote binding to Fgn [54]. Protein co-deposition also reduced the antibacterial activities of the Ag and AgF-2 as dead cells were not found on surfaces. This is consistent with the ICP results. Taken together, these data suggest that (1) bacterial interactions with host-derived proteins, particularly Fgn, increased the ability of bacterial adhesion and biofilm formation; (2) the antibacterial activity of Ag-based coatings was reduced due to protein adsorption; (3) the AgFP can effectively inhibit biofilm formation even in the presence of proteins due to its superior surface repellence.

### 3.6. XDLVO modelling

To gain more insight into the adhesion behaviour of bacteria and proteins on different surfaces, the interaction energy ($\Delta E^{TOT}$) as a function of separation distance (H) was calculated using the XDLVO model (see Supporting Information for details) [18,55]. In the case of *E. coli*, Fig. 6a shows that the XDLVO predicted a clear attractive secondary minimum at about 8 nm for the SS, Ag, and AgF-1 surfaces prior to entering a strongly repulsive region, which could allow bacteria to adhere reversibly. Similar results were also obtained with *S. aureus*. However, the $\Delta E^{TOT}$ values of the AgF-2, AgF-3, and AgFP remained positive regardless of H. Bacteria at a large distance are attracted towards the surfaces mainly *via* Lifshitz-van der Waals (LW) forces, while the presence of PTFE resulted in a significant decrease in the $\Upsilon_s^{LW}$, and this consequently led to a positive value of the Lifshitz-van der Waals interaction energy ($\Delta E^{LW}$) according to eq. (3):

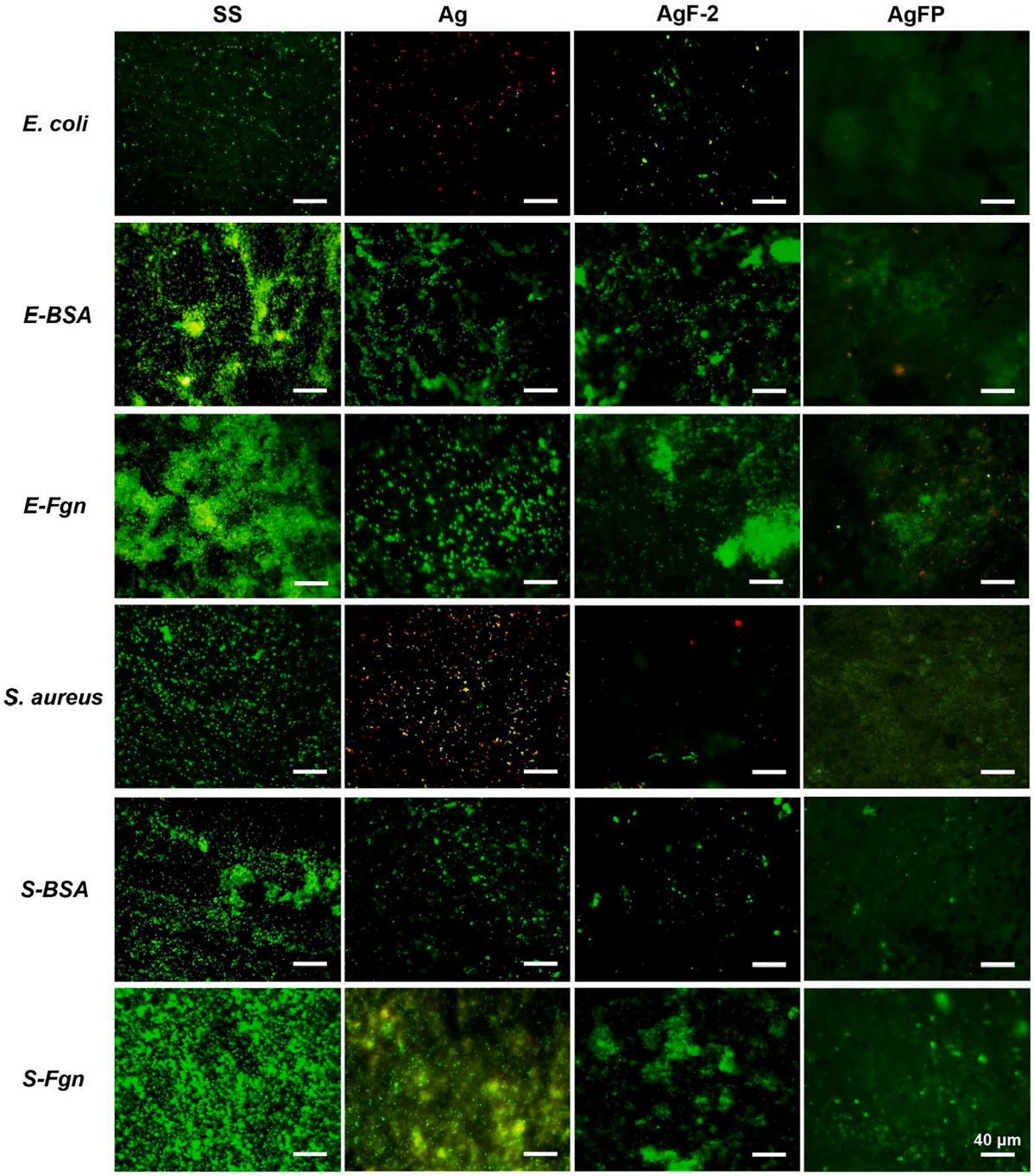


**Fig. 5.** Live/dead assay: fluorescence microscope images of *E. coli* and *S. aureus* on the SS, Ag, AgF-2, and AgFP after 1-day co-culture in different media. Typical images are shown from one of several examinations (scale bars correspond to 40 μm).

$$\Delta E^{LW} = -\frac{24\pi R H_0^2\left(\sqrt{\gamma_p^{LW}} - \sqrt{\gamma_f^{LW}}\right)\left(\sqrt{\gamma_s^{LW}} - \sqrt{\gamma_f^{LW}}\right)}{6H} \quad (3)$$

where $H_0$ is the minimum equilibrium distance (0.157 nm) between the two interacting surfaces [55]. This indicates that incorporating PTFE into the Ag coating could reduce the likelihood of bacteria attachment as more bacteria would be trapped within a deeper secondary energy minimum. Upon close approach (<1 nm), the Lewis acid-base (AB) interactions, which describe attractive hydrophobic or repulsive hydrophilic repulsions, become dominant, and the ($\Delta E^{AB}$) as a function of H is shown in Fig. 6b. Despite the primary minimum not being shown, the AgF and AgFP coatings with a higher hydrophobic character exhibited a lower energy barrier at close contact, suggesting that the reversibly attached bacteria on the AgF or AgFP coating would likely become irreversibly attached due to hydrophobic attraction. This was verified by the adhesion results since more bacteria became attached to the AgF-3 than AgF-1 and AgF-2 (Fig. 4b). However, this finding does not comply with the AgFP as cell clusters or biofilm were not observed using fluorescent microscopy (Fig. 5).

As for protein adsorption (e.g., BSA), Fig. 6c shows both primary minimum and secondary minimum, suggesting that BSA could easily escape the barrier and become irreversibly attached. Similar to bacterial adhesion, the presence of hydrophobic PTFE or the liquid-like overlayer increased the energy barrier at the secondary energy minimum for reversible protein adhesion but enhanced irreversible adsorption at

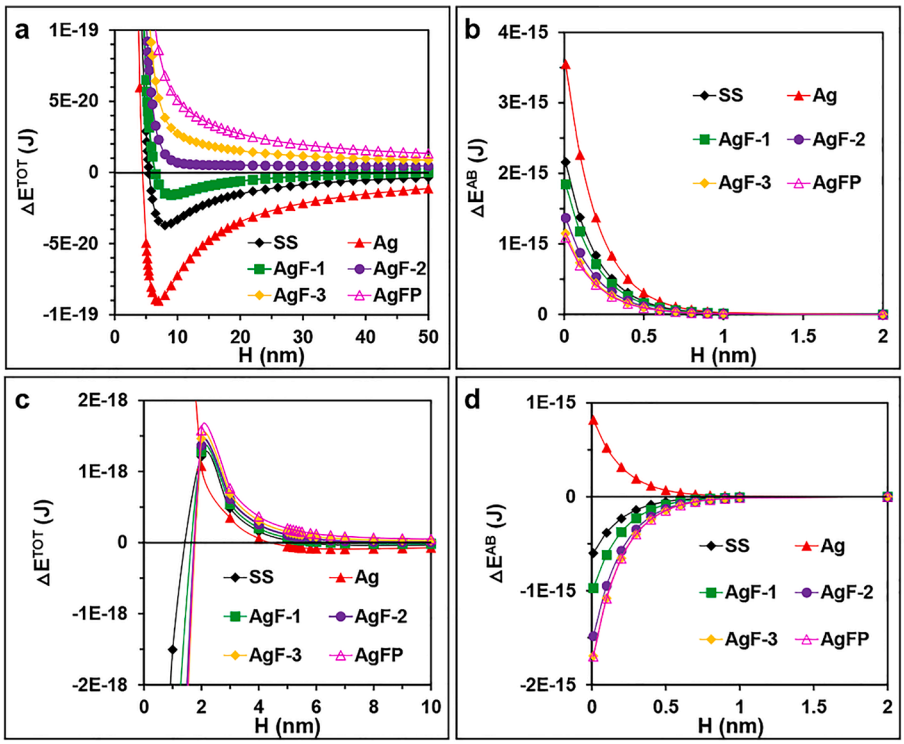


**Fig. 6.** XDLVO modelling of bacterial adhesion and protein adsorption. Effects of separation distance (H) on (a) total interaction energy and (b) Lewis acid-base interaction energy between *E. coli* and surfaces; Effects of H on (c) total interaction energy and (d) Lewis acid-base interaction energy between BSA and surfaces.

close contact (Fig. 6d). For the Ag coating, despite its hydrophilic feature predicting a strong repulsion against protein within 1 nm, its deep secondary energy minimum allowed more reversible protein adsorption and the proteins may rearrange or adjust their structures to attach to the surfaces as protein has both hydrophilic and hydrophobic segments. Taken together, the XDLVO model could be used to predict and explain the adhesion of bacteria and protein to traditional surfaces, whereas the interaction between the AgFP coating and bacteria/protein was more complicated due to its self-cleaning feature. Other factors such as surface chemistry, surface roughness, and environment have also been extensively reported to influence protein adsorption, making it an open field for extensive research in the future.

### 3.7. Cytotoxicity assay

The cytocompatibility of the coatings was assessed with L929 mouse fibroblasts. As shown in Fig. 7, the SS group showed the highest cell viability (CV) over the test period demonstrating no significance ($p > 0.05$) relative to the control after 1 day of immersion. A slight decrease was noticed after 3 days of co-incubation, which could be ascribed to the release of a trace amount of metal ions such as chromium and nickel considering that the electropolishing step destroyed the oxidative film on SS surfaces. In comparison, the Ag and AgF-2 coating showed a significant decline in CV when compared with the control ($p < 0.05$) and the values of CV decreased with immersion time, suggesting that the use of traditional Ag or AgF coating for indwelling devices with a large surface may lead to compromised biocompatibility despite only trace amounts of silver being released. In comparison, the AgFP group exhibited a higher CV as compared with the Ag and AgF-2 groups and cumulative toxicity was not observed with immersion time. Combined with the ICP results (Fig. 4a), the AgFP demonstrated a significant advantage as the coating functions mainly *via* the liquid-like layer instead of releasing silver, and this could account for the improved cytocompatibility.

The cell morphologies after incubating with different samples were

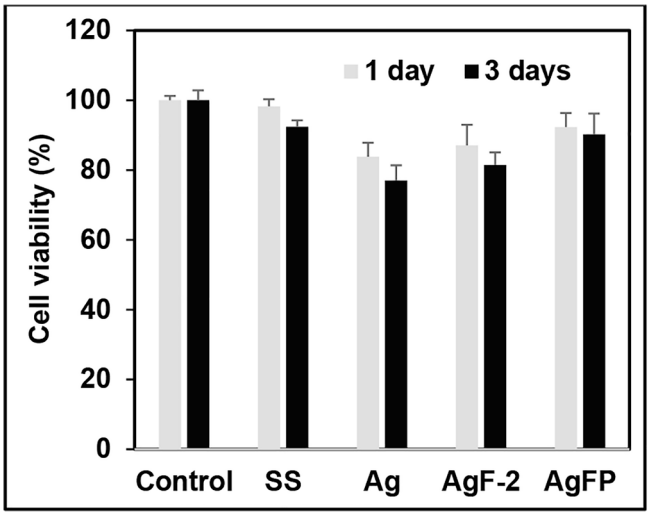


**Fig. 7.** Cell viability after contacting with samples (n = 6, bars are standard error of the mean).

compared by confocal microscopy (Fig. 8). The cells in control, SS, and AgFP groups displayed healthy spindle-like morphology and the cell nuclei indicated by DAPI staining showed full integrity. In comparison, cells after incubating with the Ag and AgF-2 surfaces were induced to round up, but no obvious morphological damage was noticed. A slight decrease in cell density was noticed as compared with the control, which is consistent with the MTT result. These findings suggested that the AgFP coating exerted no significant toxicity at this stage. However, further evaluation may be required to understand the long-term cell responses toward the coatings.

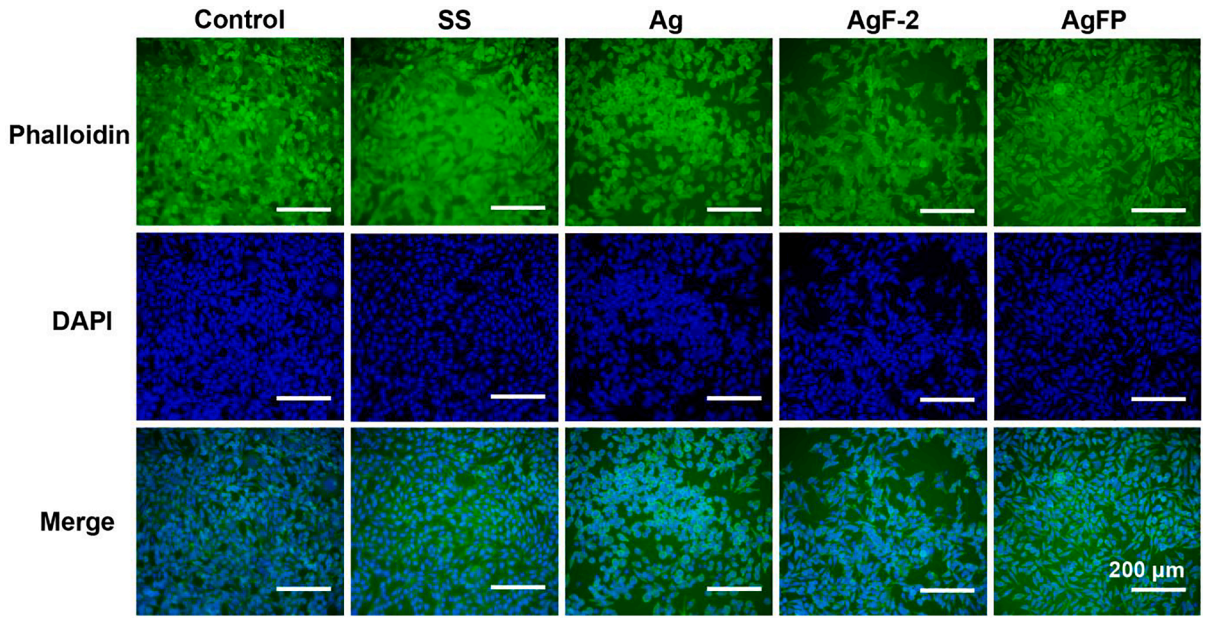


**Fig. 8.** Fluorescence images of L929 cells after 72 h of incubation with different samples (scale bar corresponds to 200 μm). Typical images are shown from one of several examinations.

## 4. Conclusions

In summary, we have described a simple procedure to fabricate a liquid-like AgF-based coating for medical devices and demonstrated its feasibility to prevent bacteria-protein-associated biofilm formation. This procedure is based on the hydrolysis and polycondensation of PFOTES in combination with a capillary lock-in action, which leads to the formation of a smooth and slippery layer over the AgF coatings. The prepared AgFP coating exhibited outstanding repellence against liquids with a broad range of surface tensions and maintained good long-term stability in aqueous conditions. Compared with traditional Ag and AgF coatings, the AgFP coating showed ultralow adhesion for both bacteria and proteins. Protein-bacteria co-deposition experiments showed that the AgFP coating was able to significantly inhibit biofilm formation in near-real conditions. The cytotoxicity assay also demonstrated that the AgFP was non-toxic with fibroblast cells. Taken together, the results indicate that the liquid-like AgFP coating with excellent self-cleaning properties could be a promising candidate for use in medical devices to combat infections. However, it should be noted that the self-cleaning function of the coating should be tested in a complex physiologically relevant environment (e.g., an animal model) to further confirm its function.

*CRediT authorship contribution statement*

**Shuai Zhang:** Conceptualization, Methodology, Validation, Investigation, Resources, Writing – original draft. **Xinjin Liang:** Conceptualization, Methodology, Validation, Investigation. **Xiao Teng:** Investigation, Data curation. **Geoffrey M. Gadd:** Visualization, Writing – review & editing. **John W. McGrath:** Supervision, Writing – review & editing. **Coin P. McCoy:** Resources, Writing – review & editing. **Qi Zhao:** Visualization, Supervision, Writing – review & editing, Resources.

## Declaration of Competing Interest

The authors declare that they have no known competing financial interests or personal relationships that could have appeared to influence the work reported in this paper.

## Data availability

Data will be made available on request.

## Acknowledgements

We acknowledge Dr. Alina Schilling for SEM and EDX analysis.

## Appendix A. Supplementary material

Supplementary data to this article can be found online at https://doi.org/10.1016/j.apsusc.2023.156463.

## References

[1] W.M.J. Dunne, Bacterial adhesion: seen any good biofilms lately? Clin. Microbiol. Rev. 15 (2) (2002) 155–166.
[2] Z.K. Zander, M.L. Becker, Antimicrobial and antifouling strategies for polymeric medical devices, ACS Macro Lett. 7 (1) (2018) 16–25.
[3] K. Chae, W.Y. Jang, K. Park, J. Lee, H. Kim, K. Lee, C.K. Lee, Y. Lee, S.H. Lee, J. Seo, Antibacterial infection and immune-evasive coating for orthopedic implants, Sci. Adv. 6 (44) (2020) eabb0025.
[4] R. Greenhalgh, N.C. Dempsey-Hibbert, K.A. Whitehead, Antimicrobial strategies to reduce polymer biomaterial infections and their economic implications and considerations, Int. Biodeterior. Biodegradation 136 (2019) 1–14.
[5] S. Zhang, X. Liang, G.M. Gadd, Q. Zhao, Marine microbial-derived antibiotics and biosurfactants as potential new agents against catheter-associated urinary tract infections, Mar. Drugs. 19 (5) (2021) 255.
[6] M.E. Rupp, T. Fitzgerald, N. Marion, V. Helget, S. Puumala, J.R. Anderson, P. D. Fey, Effect of silver-coated urinary catheters: efficacy, cost-effectiveness, and antimicrobial resistance, Am. J. Infect. Control. 32 (8) (2004) 445–450.
[7] M. Riool, A. de Breij, J.W. Drijfhout, P.H. Nibbering, S.A.J. Zaat, Antimicrobial peptides in biomedical device manufacturing, Front. Chem. 5 (2017) 63.
[8] B. Thallinger, E.N. Prasetyo, G.S. Nyanhongo, G.M. Guebitz, Antimicrobial enzymes: an emerging strategy to fight microbes and microbial biofilms, Biotechnol. J. 8 (1) (2013) 97–109.
[9] K.H. Homeyer, M.J. Goudie, P. Singha, H. Handa, Liquid-infused nitric-oxide-releasing silicone foley urinary catheters for prevention of catheter-associated urinary tract infections, ACS Biomater. Sci. Eng. 5 (4) (2019) 2021–2029.
[10] N. Nikfarjam, M. Ghomi, T. Agarwal, M. Hassanpour, E. Sharifi, D. Khorsandi, M. Ali Khan, F. Rossi, A. Rossetti, E. Nazarzadeh Zare, N. Rabiee, D. Afshar, M. Vosough, T. Kumar Maiti, V. Mattoli, E. Lichtfouse, F.R. Tay, P. Makvandi, Antimicrobial ionic liquid-based materials for biomedical applications, Adv. Funct. Mater. 31 (42) (2021) 2104148.
[11] P. Singha, J. Locklin, H. Handa, A review of the recent advances in antimicrobial coatings for urinary catheters, Acta Biomater. 50 (2017) 20–40.
[12] L. Wang, T.J. McCarthy, Covalently attached liquids: instant omniphobic surfaces with unprecedented repellency, Angew. Chem. Int. Ed. 55 (1) (2016) 244–248.

[13] S. Zheng, M. Bawazir, A. Dhall, H.-E. Kim, L. He, J. Heo, G. Hwang, implication of surface properties, bacterial motility, and hydrodynamic conditions on bacterial surface sensing and their initial adhesion, Front. Bioeng. Biotechnol. 9 (2021), 643722.

[14] M. Hermansson, The DLVO theory in microbial adhesion, Colloids Surf. B. 14 (1) (1999) 105–119.

[15] Y.H. An, R.J. Friedman, Concise review of mechanisms of bacterial adhesion to biomaterial surfaces, J. Biomed. Mater. Res. 43 (3) (1998) 338–348.

[16] Y. Cheng, G. Feng, C.I. Moraru, Micro- and nanotopography sensitive bacterial attachment mechanisms: a review, Front. Microbiol. 10 (2019) 191.

[17] R.E. Baier, Substrata influences on adhesion of microorganisms and their resultant new surface properties. Adsorpt. Microorg. Surf. (1980) 59–104.

[18] Q. Zhao, Effect of surface free energy of graded NI-P-PTFE coatings on bacterial adhesion, Surf. Coat. Technol. 185 (2–3) (2004) 199–204.

[19] C.M. Magin, S.P. Cooper, A.B. Brennan, Non-toxic antifouling strategies, Mater. Today 13 (4) (2010) 36–44.

[20] Q. Zhao, Y. Liu, C. Wang, Development and evaluation of electroless Ag-PTFE composite coatings with anti-microbial and anti-corrosion properties, Appl. Surf. Sci. 252 (5) (2005) 1620–1627.

[21] S. Zhang, L. Wang, X. Liang, J. Vorstius, R. Keatch, G. Corner, G. Nabi, F. Davidson, G.M. Gadd, Q. Zhao, Enhanced antibacterial and antiadhesive activities of silver-PTFE nanocomposite coating for urinary catheters, ACS Biomater. Sci. Eng. 5 (6) (2019) 2804–2814.

[22] J. Palmer, S. Flint, J. Brooks, Bacterial cell attachment, the beginning of a biofilm, J. Ind. Microbiol. Biotechnol. 34 (9) (2007) 577–588.

[23] M. Talha, Y. Ma, P. Kumar, Y. Lin, A. Singh, Role of protein adsorption in the bio corrosion of metallic implants - a review, Colloids Surf. B. 176 (2019) 494–506.

[24] M.J. Andersen, C. Fong, A.A. la Bella, J.J. Molina, A. Molesan, M.M. Champion, C. Howell, A.L. Flores-Mireles, Inhibiting host-protein deposition on urinary catheters reduces associated urinary tract infections, Elife 11 (2022) e75798.

[25] V. Panchalingam, B. Poon, H.H. Huo, C.R. Savage, R.B. Timmons, R.C. Eberhart, Molecular surface tailoring of biomaterials via pulsed RF plasma discharges, J. Biomater. Sci. Polym. Ed. 5 (1–2) (1993) 131–145.

[26] G. Zardeneta, H. Mukai, V. Marker, S.B. Milam, Protein interactions with particulate Teflon: implications for the foreign body response, J. Oral Maxillofac. Surg. 54 (7) (1996) 873–878.

[27] T.S. Wong, S.H. Kang, S.K.Y. Tang, E.J. Smythe, B.D. Hatton, A. Grinthal, J. Aizenberg, Bioinspired self-repairing slippery surfaces with pressure-stable omniphobicity, Nature 477 (7365) (2011) 443–447.

[28] C. Wei, G. Zhang, Q. Zhang, X. Zhan, F. Chen, Silicone oil-infused slippery surfaces based on sol-gel process-induced nanocomposite coatings: a facile approach to highly stable bioinspired surface for biofouling resistance, ACS Appl. Mater. Interfaces 8 (2016) 34810–34819.

[29] E. Ozkan, A. Mondal, M. Douglass, S.P. Hopkins, M. Garren, R. Devine, R. Pandey, J. Manuel, P. Singha, J. Warnock, H. Handa, Bioinspired ultra-low fouling coatings on medical devices to prevent device-associated infections and thrombosis, J. Colloid Interface Sci. 608 (2022) 1015–1024.

[30] J. Chen, C. Howell, C.A. Haller, M.S. Patel, P. Ayala, K.A. Moravec, E. Dai, L. Liu, I. Sotiri, M. Aizenberg, J. Aizenberg, E.L. Chaikof, An immobilized liquid interface prevents device associated bacterial infection in vivo, Biomaterials 113 (2017) 80–92.

[31] Y. Chan, X.H. Wu, B.W. Chieng, N.A. Ibrahim, Y.Y. Then, Superhydrophobic nanocoatings as intervention against biofilm-associated bacterial infections, Nanomaterials 11 (2021) 1046.

[32] Y. Lu, S. Sathasivam, J. Song, C.R. Crick, C.J. Carmalt, I.P. Parkin, Repellent materials. Robust self-cleaning surfaces that function when exposed to either air or oil, Science 347 (6226) (2015) 1132–1135.

[33] W. Li, X. Tang, X. Han, J. Li, Y. Chu, L. Wang, Super-alcohol-repellent coatings, J. Colloid Interface Sci. 613 (2022) 146–154.

[34] J. Guerin, Bath composition for electropolishing of titanium and method for using same, US 6 610 194 B1. (2003).

[35] R. Guo, G. Yin, X. Sha, Q. Zhao, L. Wei, H. Wang, The significant adhesion enhancement of Ag-polytetrafluoroethylene antibacterial coatings by using of molecular bridge, Appl. Surf. Sci. 341 (2015) 13–18.

[36] C.J. van Oss, R.J. Good, M.K. Chaudhury, The role of van der Waals forces and hydrogen bonds in “hydrophobic interactions” between biopolymers and low energy surfaces, J. Colloid Interface Sci. 111 (2) (1986) 378–390.

[37] J.R. Wiśniewski, F.Z. Gaugaz, Fast and sensitive total protein and Peptide assays for proteomic analysis, Anal Chem. 87 (2015) 4110–4116.

[38] S. Zhang, X. Liang, G.M. Gadd, Q. Zhao, A sol-gel based silver nanoparticle/polytetrafluorethylene (AgNP/PTFE) coating with enhanced antibacterial and anti-corrosive properties, Appl. Surf. Sci. 535 (2021), 147675.

[39] Y. Hua, Estimating method for electron beam accelerating voltage used in energy-dispersive X-Ray microanalysis: application in failure analysis of wafer fabrication, Instrum. Sci. Technol. 32 (2) (2004) 115–126.

[40] P. Rodič, J. Iskra, I. Milošev, A hybrid organic-inorganic sol-gel coating for protecting aluminium alloy 7075–T6 against corrosion in Harrison’s solution, J. Sol-Gel Sci. Technol. 70 (1) (2014) 90–103.

[41] C.G.L. Furmidge, Studies at phase interfaces. I. The sliding of liquid drops on solid surfaces and a theory for spray retention, J. Colloid Sci. 17 (4) (1962) 309–324.

[42] J. Jiang, H. Zhang, W. He, T. Li, H. Li, P. Liu, M. Liu, Z. Wang, Z. Wang, X. Yao, Adhesion of microdroplets on water-repellent surfaces toward the prevention of surface fouling and pathogen spreading by respiratory droplets, ACS Appl. Mater. Interfaces 9 (2017) 6599–6608.

[43] T.G. Papaioannou, C. Stefanadis, Vascular wall shear stress: basic principles and methods, Hellenic. J. Cardiol. 46 (1) (2005) 9–15.

[44] B. Zalewska-Piątek, M. Olszewski, T. Lipniacki, S. Błoński, M. Wieczór, P. Bruździak, A. Skwarska, B. Nowicki, S. Nowicki, R. Piątek, A shear stress micromodel of urinary tract infection by the Escherichia coli producing Dr adhesin, PLoS Pathog. 16 (1) (2020) e1008247.

[45] D. Vasilaki, A. Bakopoulou, A. Tsouknidas, E. Johnstone, K. Michalakis, Biophysical interactions between components of the tumor microenvironment promote metastasis, Biophys Rev. 13 (3) (2021) 339–357.

[46] B. Molleman, T. Hiemstra, Time, pH, and size dependency of silver nanoparticle dissolution: the road to equilibrium, Environ. Sci. Nano. 4 (6) (2017) 1314–1327.

[47] T. Misra, M. Tare, P.N. Jha, Insights into the dynamics and composition of biofilm formed by environmental isolate of enterobacter cloacae, Front. Microbiol. 13 (2022).

[48] M.A. Daeschel, J. McGuire, Interrelationships between protein surface adsorption and bacterial adhesion, Biotechnol. Genet. Eng. Rev. 15 (1998) 413–438.

[49] P. Roach, D. Farrar, C.C. Perry, Interpretation of protein adsorption: surface-induced conformational changes, J. Am. Chem. Soc. 127 (22) (2005) 8168–8173.

[50] X. Wang, G. Herting, I. Odnevall Wallinder, E. Blomberg, Adsorption of bovine serum albumin on silver surfaces enhances the release of silver at pH neutral conditions, Phys. Chem. Chem. Phys. 17 (28) (2015) 18524–18534.

[51] J.E. Kinsella, D.M. Whitehead, Proteins in whey: chemical, physical, and functional properties, Adv. Food Nutr. Res. 33 (1989) 343–438.

[52] D.R. Absolom, C.J. van Oss, W. Zingg, A.W. Neumann, Determination of surface tensions of proteins II. Surface tension of serum albumin, altered at the protein-air interface, Biochim. Biophys. Acta. 670 (1) (1981) 74–78.

[53] J.L. Yu, R. Andersson, A. Ljungh, Protein adsorption and bacterial adhesion to biliary stent materials, J. Surg. Res. 62 (1) (1996) 69–73.

[54] P. Herman-Bausier, C. Labate, A.M. Towell, S. Derclaye, J.A. Geoghegan, Y. F. Dufrêne, *Staphylococcus aureus* clumping factor A is a force-sensitive molecular switch that activates bacterial adhesion, Proc. Natl. Acad. Sci. 115 (21) (2018) 5564–5569.

[55] W. Funke, Interfacial forces in aqueous media, Prog. Org. Coat. 26 (1995) 75–76.

[56] S. Zhang, X. Liang, G.M. Gadd, Q. Zhao, Advanced titanium dioxide-polytetrafluorethylene ($TiO_2$-PTFE) nanocomposite coatings on stainless steel surfaces with antibacterial and anti-corrosion properties, Appl. Surf. Sci. 490 (2019) 231–241.